
Grounding Bodily Awareness in Visual Representations for Efficient Policy Learning

Junlin Wang

SUSTech

Shenzhen, China

12112921@mail.sustech.edu.cn

Zhiyun Lin

SUSTech

Shenzhen, China

linzy@sustech.edu.cn

Abstract

Learning effective visual representations for robotic manipulation remains a fundamental challenge due to the complex body dynamics involved in action execution. In this paper, we study how visual representations that carry body-relevant cues can enable efficient policy learning for downstream robotic manipulation tasks. We present **Inter-token Contrast (Icon)**, a contrastive learning method applied to the token-level representations of Vision Transformers (ViTs). Icon enforces a separation in the feature space between agent-specific and environment-specific tokens, resulting in agent-centric visual representations that embed body-specific inductive biases. This framework can be seamlessly integrated into end-to-end policy learning by incorporating the contrastive loss as an auxiliary objective. Our experiments show that Icon not only improves policy performance across various manipulation tasks but also facilitates policy transfer across different robots. The project website: <https://inter-token-contrast.github.io/icon/>

1 Introduction

Vision serves not only the awareness of the external environment but also the awareness of one’s own self [11]. Through vision, we perceive our bodies, monitor our movements, and maintain a perceptual boundary between self and non-self. This form of bodily awareness, commonly referred to as *visual proprioception* [2], enables agents to respond to their own bodily dynamics in a flexible and adaptive manner. Such responsiveness is essential for planning and executing actions in tasks that require high-level action sensitivity, such as locomotion and manipulation [10]. Going further, incorporating such inductive biases, particularly those arising from the agent’s body within the visual field, can be highly beneficial to learning policies for robotic tasks [12, 17, 39]. With awareness of the position and movement of its own body, a robotic agent can efficiently learn structured agent-environment representations from raw pixel observations [12].

However, despite existing efforts in visuomotor policy learning, extracting body-aware information from high-dimensional images remains challenging, especially in end-to-end learning frameworks where visual encoders are jointly optimized with policy networks [24]. Since both components share the same optimization objective, models can easily converge to bottlenecks that inadvertently filter out task-irrelevant cues, including visual signals related to the agent’s body. This issue becomes even more pronounced when training data is deficient. To address this, one approach is to augment the policy loss with an agent-centric auxiliary objective [12, 29]. These methods typically involve reconstructing RGB observations or agent masks from latent representations to implicitly disentangle a robotic agent from its environment. While this strategy has proven effective across various tasks, we argue that the reconstruction loss can undermine the training stability of policy learning. This raises a key question: is there a more natural way to derive disentangled agent-environment representations from pixels without sacrificing model performance and training stability?

To this end, we propose **Inter-token Contrast (Icon)**, a contrastive learning approach designed to extract agent-centric representations from the Vision Transformer (ViT) [8], a high-capacity visual encoder widely utilized in robotic manipulation [9, 19, 32, 42]. Icon applies contrastive learning to the ViT’s token-level features, where features corresponding to the agent are pulled together, and are contrasted against those corresponding to the environment, and vice versa. By explicitly decoupling agent-specific and agent-agnostic features, we implicitly encourage the model to focus on agent-relevant information, rather than information of the entire scene. We further introduce the following technical contributions to enhance the performance of Icon:

- We bring Farthest Point Sampling (FPS) [30] into 2D domains to sample keys from tokens for contrastive learning. By encouraging a wide spatial distribution of keys, FPS ensures that the selected features capture diverse and informative aspects of either the agent or the environment, maintaining a good representation of the overall structure.
- We propose a multi-level design that fuses inter-token contrastive losses from multiple layers of the ViT encoder, enabling a more complete disentanglement between the agent and its environment within the learned visual representations.

Through extensive experiments, we demonstrate that integrating Icon with Diffusion Policy [5], a state-of-the-art imitation learning algorithm, leads to consistent performance improvements across 8 manipulation tasks spanning 3 different robots from 2 benchmarks. Code, data, and videos can be found: <https://inter-token-contrast.github.io/icon/>

2 Related work and background

2.1 Visuomotor policy learning

Training control policies that map visual sensory inputs directly to motor actions has been widely studied in reinforcement learning (RL) [21, 24, 44] and imitation learning (IL) [5, 23, 26, 37]. Among all, several works have explored learning improved representations for visual control through auxiliary tasks. Dasari and Gupta [7] leverage learned representations to predict the gripper’s future location as a 2D keypoint in the image for debugging purposes, although they do not explicitly use this auxiliary objective for representation learning. Extending this line of work, Yarats et al. [45] couple a policy network with an autoencoder to reconstruct raw image pixels from the learned latent space, which has proven effective to improve the sample efficiency of RL algorithms. Building upon this idea, Gmelin et al. [12] incorporate an additional autoencoder to reconstruct binary agent masks, yielding an agent-centric representation that facilitates policy transfer across different robots. More recently, Li et al. [25] introduce the reconstruction approach to the reverse diffusion process [16], where a decoder reconstructs both pixel and state information from the intermediate representations of a U-Net model [34] to enhance the performance of a diffusion-based policy [5]. Our approach is similar to Laskin et al. [22] and Zhu et al. [47], which augment the policy objective with an auxiliary contrastive loss. However, instead of focusing on extracting task-relevant semantics from high-dimensional images, we aim to explicitly encourage the policy to develop a bodily awareness within the learned visual representations.

2.2 Contrastive learning

Contrastive learning is a self-supervised learning paradigm to learn useful representations from high-dimensional data, such as natural language [31], images [3, 4, 15, 31], and videos [27, 36, 43]. It can be interpreted as training an encoder for a dictionary look-up task, whose goal is to pull the query closer to a positive key while pushing it away from all other negative keys. This is typically achieved by minimizing a contrastive loss [6], which serves as an unsupervised objective function for training the encoder networks. Commonly used contrastive losses include Triplet loss [35], N-pair loss [38], Noise Contrastive Estimation (NCE) loss [13], and InfoNCE loss [28]. In this paper, we adopt a variant of the InfoNCE loss proposed by Wang et al. [41]:

$$\mathcal{L}_{\text{InfoNCE}}(q, \mathcal{K}^+, \mathcal{K}^-) = \frac{1}{|\mathcal{K}^+|} \sum_{k^+ \in \mathcal{K}^+} -\log \frac{\exp(q \cdot k^+ / \tau)}{\exp(q \cdot k^+ / \tau) + \sum_{k^- \in \mathcal{K}^-} \exp(q \cdot k^- / \tau)}, \quad (1)$$

where q , \mathcal{K}^+ , and \mathcal{K}^- denote the query, the set of positive keys, and the set of negative keys, respectively; (\cdot) denotes the dot product; and τ is a temperature hyperparameter.

3 Visually grounded agent-centric representations

In principle, it is possible to integrate ICon with any visuomotor policy that uses vision transformers as visual encoders. In this section, we begin with an overview of the vanilla vision transformer, followed by a detailed explanation of the key design choices of ICon as well as its integration with a policy network. An overview of ICon is shown in Figure 1.

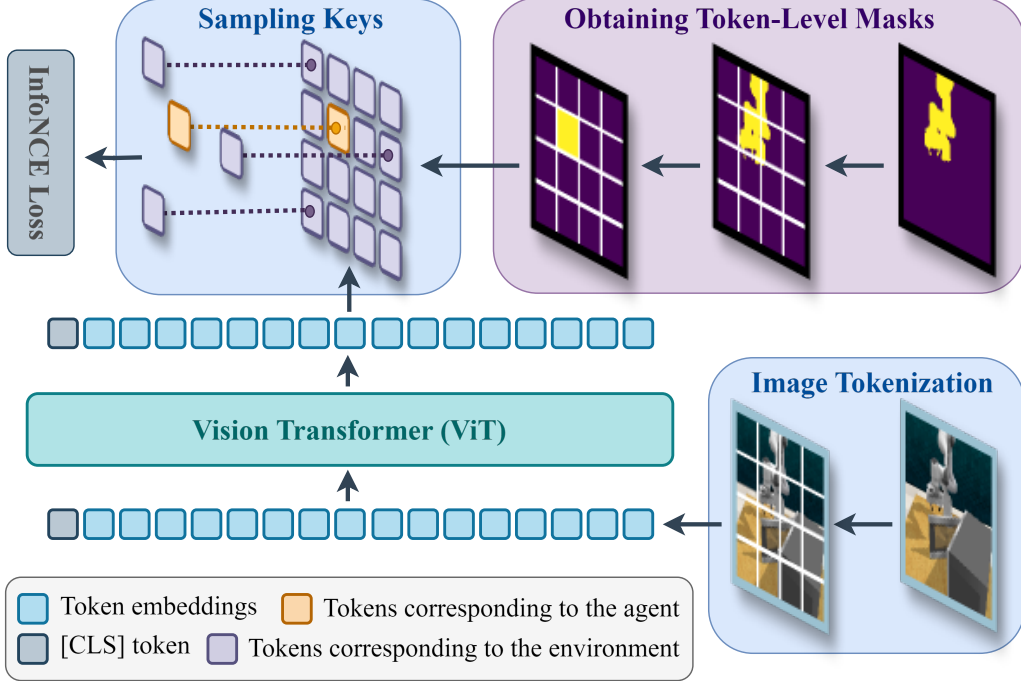


Figure 1: Overview of ICon. A full-scene RGB image containing a robotic agent is tokenized and processed by a vision transformer. The resulting token-level features (excluding the [CLS] token) are reshaped and aligned with a token-level mask derived from the agent’s segmentation mask. Tokens corresponding to the agent and the environment are then sampled and used as keys to compute the inter-token contrastive loss.

3.1 Preliminaries: vision transformers

Vision Transformers (ViTs) [8] extract token-level representations from high-dimensional images. As depicted in Figure 1, an image $\mathcal{I} \in \mathbb{R}^{H \times W \times 3}$ is first divided into non-overlapping patches, each of size $P \times P$, and then embedded into a sequence of tokens $\mathcal{T} \in \mathbb{R}^{N \times D}$, where $N = HW/P^2$ denotes the number of patches and D is the embedding dimension. The token embeddings, prepended with a learnable classification token [CLS], are subsequently fed into the ViT encoder to produce a sequence of token-level features $[\mathcal{F}_{\text{cls}}, \mathcal{F}]$, where $\mathcal{F}_{\text{cls}} \in \mathbb{R}^D$ and $\mathcal{F} \in \mathbb{R}^{N \times D}$ correspond to the [CLS] token and the patch embeddings, respectively.

3.2 Token-level agent masks

While we have obtained token-level features from the vision transformer, how can we determine which features are agent-specific and which are agent-agnostic? Recall that each token corresponds to an image patch consisting of a set of pixels. Each pixel can be classified as belonging to either the agent or the environment based on an agent mask [12, 17, 29]. Therefore, we can propagate these pixel-level assignments to the token level.

Specifically, given the image \mathcal{I} of the full scene, we use a segmentation model to generate a binary mask $\mathcal{M} \in \mathbb{R}^{H \times W}$, where $\mathcal{M}_{i,j} = 1$ for pixels occupied by the agent and 0 otherwise. This mask \mathcal{M}

is then patchified into $\mathcal{P}_{\text{mask}} = \{p_{k,l}\}_{k=1,l=1}^{H/P,W/P}$ following the same patchification procedure applied to the image \mathcal{I} in ViT encoding. Since each patch $p_{k,l}$ may contain a mix of agent-related and environment-related pixels, we determine its dominant class based on a masking threshold $\beta \in [0, 1]$: if the proportion of agent pixels in a patch exceeds β , the patch is considered agent-dominated and assigned a value of 1; otherwise, it is considered environment-dominated and assigned a value of 0 (Equation (2)). This yields a new patch-level (or token-level) mask $\mathcal{M}_{\text{token}} = \{m_{k,l}\}_{k=1,l=1}^{H/P,W/P}$, where $m_{k,l} \in \{0, 1\}$.

$$m_{k,l} = \begin{cases} 1 & \text{if } \text{sum}(p_{k,l}) > \beta P^2 \\ 0 & \text{otherwise} \end{cases}. \quad (2)$$

3.3 Inter-token contrastive loss

Now that we have acquired the token-level features and the agent masks, we introduce an inter-token contrastive loss to help the model distinguish between the agent and its environment. Our intuition is straightforward: features that belong to the same class (agent or environment) should be similar, while features coming from different classes should be dissimilar. To fulfill this, we encourage features of the same class to cluster together while enforcing separation between features of different classes, resulting in a clearer boundary between the agent and its environment in the learned feature space.

Specifically, given the token-level features \mathcal{F} and the corresponding agent masks $\mathcal{M}_{\text{token}}$, we first rearrange the sequence-like features \mathcal{F} into a 2D feature map $\mathcal{F}_{\text{map}} = \{f_{k,l}\}_{k=1,l=1}^{H/P,W/P}$ for subsequent processing. We then compute the agent-specific query q_a and environment-specific query q_e by averaging the corresponding features, as defined in Equation 3, where $\mathbb{I}(\cdot)$ stands for the indicator function. As for key selection, we adapt the Farthest Point Sampling (FPS) method [30] from point cloud sampling to the 2D domain (see Algorithm 1). Compared with random sampling, FPS promotes diversity through selecting points that are spatially well-distributed (see Figure 2), ensuring that the sampled keys capture diverse and representative features of the agent and the environment. By applying FPS within the feature map \mathcal{F}_{map} while restricting sampling regions using $\mathcal{M}_{\text{token}}$ and $(1 - \mathcal{M}_{\text{token}})$, we obtain a set of agent-specific keys \mathcal{K}_a and a set of environment-specific keys \mathcal{K}_e , respectively. Note that for the agent-specific query q_a , the agent-specific keys \mathcal{K}_a serve as positive keys, while the environment-specific keys \mathcal{K}_e serve as negative keys, and vice versa for the environment-specific query q_e . Finally, we compute two symmetric InfoNCE losses (Equation 1) for the queries using their respective positive and negative keys, and combine them together to form the ICon objective (see Equation 4). The complete pseudocode for ICon is provided in Algorithm 2 of Appendix D.

$$q_a = \frac{1}{\text{sum}(\mathcal{M}_{\text{token}})} \sum_{k=1}^{H/P} \sum_{l=1}^{W/P} \mathbb{I}(m_{k,l} = 1) f_{k,l}, \quad (3)$$

$$q_e = \frac{1}{\text{sum}(1 - \mathcal{M}_{\text{token}})} \sum_{k=1}^{H/P} \sum_{l=1}^{W/P} \mathbb{I}(m_{k,l} = 0) f_{k,l}.$$

$$\mathcal{L}_{\text{ICon}} = \mathcal{L}_{\text{InfoNCE}}(q_a, \mathcal{K}_a, \mathcal{K}_e) + \mathcal{L}_{\text{InfoNCE}}(q_e, \mathcal{K}_e, \mathcal{K}_a). \quad (4)$$

Algorithm 1 2D Farthest Point Sampling

- 1: **Input:** 2D indices $\mathcal{V} = \{(k, l)\}_{k=1,l=1}^{H,W}$, a binary mask $\mathcal{M} = \{m_{k,l} \in \{0, 1\}\}_{k=1,l=1}^{H,W}$ indicating sampling regions, number of samples N ($N \leq \sum m_{k,l}$)
 - 2: **Output:** Indices of samples \mathcal{V}'
 - 3: $\mathcal{D} \leftarrow \{d_{k,l} = \infty\}_{k=1,l=1}^{H,W}$ \triangleright Distance map
 - 4: Randomly select (\tilde{k}, \tilde{l}) where $m_{\tilde{k},\tilde{l}} = 1$
 - 5: $\mathcal{V}' \leftarrow \{(\tilde{k}, \tilde{l})\}$
 - 6: **for** $s = 1$ **to** $N - 1$ **do**
 - 7: $(\hat{k}, \hat{l}) \leftarrow \mathcal{V}'[-1]$
 - 8: **for** $k = 1$ **to** H , $l = 1$ **to** W **do**
 - 9: $\hat{d}_{k,l} \leftarrow |\hat{k} - k| + |\hat{l} - l|$
 - 10: **if** $\hat{d}_{k,l} < d_{k,l}$ **then**
 - 11: Update $d_{k,l} \leftarrow \hat{d}_{k,l}$
 - 12: **end if**
 - 13: **end for**
 - 14: $(k^*, l^*) \leftarrow \arg \max_{k,l} (m_{k,l} \cdot d_{k,l})$
 - 15: $\mathcal{V}' \leftarrow \mathcal{V}' \cup \{(k^*, l^*)\}$
 - 16: **end for**
 - 17: **return** \mathcal{V}'
-

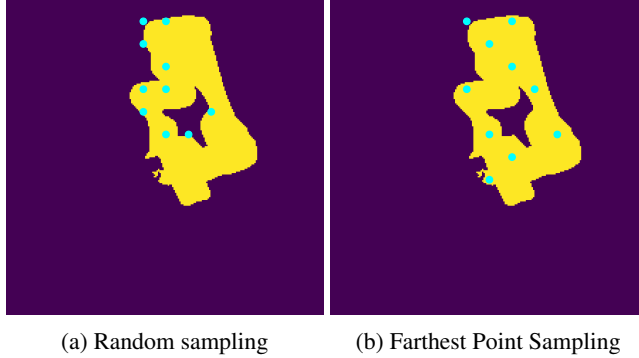


Figure 2: Visualization of point distributions sampled from the agent mask. (a) Random sampling may result in points clustered within a small region. (b) Farthest Point Sampling (FPS) produces points that are well-distributed across the entire agent.

3.4 Multi-level contrast (MLC)

In the standard ICon formulation, inter-token contrastive learning is applied only at the final layer of the vision transformer. However, we argue that this is insufficient to fully decouple the agent and its environment within the visual representations. To achieve a more complete agent-environment disentanglement, we extend ICon to each transformer encoder layer [40] of the vision transformer. Specifically, let $\mathcal{F}^{(i)}$ represent the token-level output features (excluding the [CLS] token) from the i -th layer. The inter-token contrastive loss for this layer, $\mathcal{L}_{\text{ICon}}^{(i)}$, is computed as described in Section 3.3. The overall contrastive objective is then obtained by taking a weighted sum of the layer-wise contrastive losses:

$$\mathcal{L}_{\text{ICon}} = \sum_i \frac{\exp(\gamma \cdot i)}{\sum_i \exp(\gamma \cdot i)} \mathcal{L}_{\text{ICon}}^{(i)}. \quad (5)$$

Here, γ is a hyperparameter that controls the disentangling degree across transformer encoder layers. Prior work has shown that the shallow layers of a vision transformer primarily capture positional information, while deeper layers shift toward encoding more semantic features [1]. This implies that shallower layers tend to produce more entangled agent-environment representations, resulting in larger inter-token contrastive losses. To strike a balance, we set $\gamma > 0$ to assign greater weights to the contrastive losses from deeper layers.

3.5 Training

As described above, ICon enhances a policy’s visual representations by introducing an agent-centric contrastive loss as an auxiliary objective during policy optimization. We utilize the widely adopted Diffusion Policy [5] to demonstrate how ICon can be incorporated into its training pipeline. Let $\mathcal{D} = \{(o_t \in \mathcal{O}, a_t \in \mathcal{A})\}_{t=1}^T$ denote a dataset consisting of observation-action pairs, where the observation space \mathcal{O} comprises both image observations \mathcal{I} and low-dimensional state information \mathcal{S} . Diffusion Policy learns a mapping $\pi : \mathcal{O} \rightarrow \mathcal{A}$ by training a visual encoder \mathcal{E} jointly with a diffusion model using a denoising diffusion loss $\mathcal{L}_{\text{diffusion}}$ [16]. In our framework, the visual encoder is instantiated as a vision transformer, whose output features \mathcal{F}_{cls} and \mathcal{F} are used to condition on the reverse denoising process and compute the contrastive objective $\mathcal{L}_{\text{ICon}}$, respectively. By combining the diffusion loss and the contrastive loss together with a weighting coefficient λ , we derive the following training objective for policy update:

$$\mathcal{L} = \mathcal{L}_{\text{diffusion}} + \lambda \mathcal{L}_{\text{ICon}}. \quad (6)$$

In practice, we precompute the agent masks \mathcal{M} and store them alongside the observations o_t and actions a_t in the dataset \mathcal{D} . During training, for each mini-batch sampled from \mathcal{D} , we apply identical image augmentations to the image observations and their corresponding masks before computing the training objective.

4 Experiments

We conduct a systematic evaluation of ICon across **8** manipulation tasks spanning **3** robots from 2 simulation benchmarks. Through our experiments, we seek to answer the following questions:

- 1) To what extent does ICon improve the performance of the base policy?
- 2) What are the advantages of ICon over its counterparts?
- 3) Does ICon facilitate policy transfer across different robots?
- 4) What design choices of ICon have the most influence on its performance?

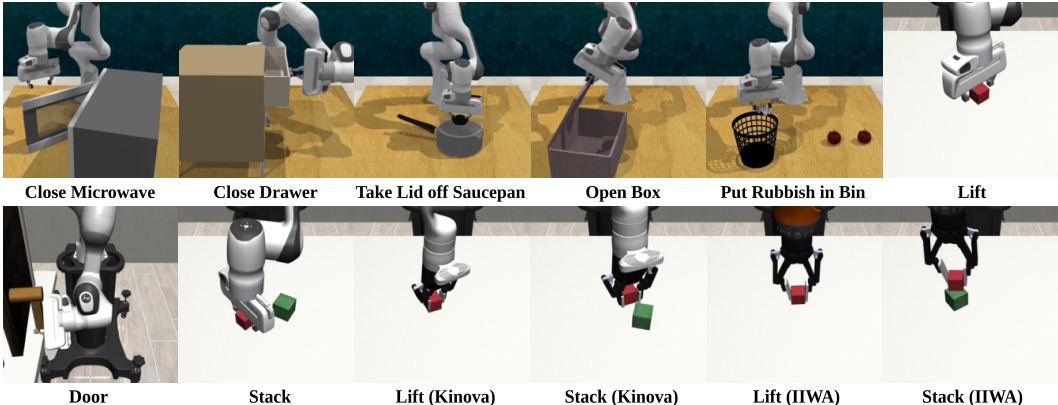


Figure 3: Visualization of simulated environments used for evaluation.

4.1 Simulation benchmarks

RLBench [18]: is a large-scale manipulation benchmark designed for meta learning, reinforcement learning, and imitation learning. It provides more than 100 robotic manipulation tasks ranging from simple target-reaching to complex long-horizon tasks. We select **5** tabletop tasks—*Close Microwave*, *Close Drawer*, *Take Lid off Saucepan*, *Open Box*, and *Put Rubbish in Bin*—which encompass object picking, articulated object manipulation, and long-horizon pick-and-place.

Robosuite [48]: is a widely used manipulation benchmark comprising 19 task environments that span both single-arm and dual-arm manipulation. From this benchmark, We select **3** representative tasks—*Lift*, *Door*, and *Stack*—which involve lifting a cube, opening a door, and stacking one cube on top of another, respectively.

4.2 Datasets

We release a new dataset covering the 8 manipulation tasks across 3 different robots in the *RLBench* and *Robosuite* environments. In *RLBench*, data are collected using the built-in motion planning toolkit, whereas in *Robosuite*, data are collected via teleoperation. Specifically, we collect **50** human demonstrations per task using a Franka Emika Panda robot, and an additional **5** demonstrations each from a Kinova Gen3 robot and a KUKA LBR IIWA robot for the *Lift* and *Stack* tasks. Each human demonstration comprises a sequence of paired observations and actions, where observations include RGB images from two viewpoints (a third-person and a wrist-mounted camera) and robot proprioception (e.g., joint position, gripper status), and actions correspond to the end-effector poses. For each RGB image, we use the Segment Anything Model (SAM) [20, 33] to extract a segmentation mask of the robot in the scene, and store the robot mask alongside the observation-action pairs in the dataset, forming a sequence of observation-mask-action triplets. In the following experiments, we train different policies using the Franka-specific data for performance comparison and fine-tune the pre-trained policies on Kinova-specific and IIWA-specific data to evaluate few-shot policy transfer across robots.

4.3 Evaluation setup

Baselines. We integrate and compare ICon with two variants of the Diffusion Policy [5]: (i) **Diff-C**, a CNN-based variant that performs well on most manipulation tasks with minimal need for hyperparameter tuning; and (ii) **Diff-T**, a transformer-based variant shown to be particularly effective for complex manipulation tasks involving frequent action changes. We refer to our methods as **ICon-Diff-C** and **ICon-Diff-T**, respectively. Additionally, we compare against Crossway Diffusion [25], which shares the same backbone as Diff-C but incorporates an auxiliary reconstruction loss to improve representation learning. For brevity, we refer to it as **Crossway-Diff-C**. To ensure a fair comparison, we also replace the ResNet [14] image encoder in the original Diff-C, Diff-T, and Crossway-Diff-C models with Vision Transformers (ViTs) [8].

Policy rollout. Before each rollout, the simulated environment is randomly initialized using a predefined seed that is consistent across all learning algorithms. At each step, instead of relying solely on the current observation to predict the next action, the policy receives the past T_o observations from the environment and predicts the next T_a actions, of which only the first T_a' are executed in the scene. In practice, we find it crucial to apply *Temporal Ensemble* [46] to the predicted action sequences to ensure smoother control and mitigate action jitters.

Evaluation methodology. We report success rates for each learning algorithm and manipulation task. Results are averaged over 3 training seeds and 50 different environment initial conditions (150 episodes in total), with standard deviations computed across the 3 training seeds. A task is considered successful if and only if the reward returned by the simulated environment changes from 0 to 1. In addition, each task has a predefined maximum number of rollout steps; if the robotic agent fails to complete the task within this limit, the episode is deemed a failure.

Table 1: Performance comparison of different algorithms on the RL Bench benchmark. We present success rates for 5 algorithms across 5 tasks in the format of (mean) \pm (standard deviation), as described in Section 4.3.

	Diff-C	Diff-T	Crossway-Diff-C	ICon-Diff-C	ICon-Diff-T
Close Microwave	0.040 \pm 0.016	0.993 \pm 0.009	0.033 \pm 0.019	0.153 \pm 0.034	1.000
Close Drawer	0.713 \pm 0.034	0.893 \pm 0.025	0.667 \pm 0.041	0.713 \pm 0.050	0.913 \pm 0.047
Take Lid off Saucepan	0.033 \pm 0.019	0.280 \pm 0.075	0.073 \pm 0.025	0.113 \pm 0.050	0.413 \pm 0.151
Open Box	0.087 \pm 0.074	0.113 \pm 0.090	0.047 \pm 0.066	0.300 \pm 0.043	0.127 \pm 0.019
Put Rubbish in Bin	0.000	0.033 \pm 0.025	0.000	0.000	0.093 \pm 0.082

Table 2: Performance comparison of different algorithms on the Robosuite benchmark. Success rates are reported for 3 algorithms across 3 tasks in the same format as in Table 1.

	Diff-C	Crossway-Diff-C	ICon-Diff-C
Lift	0.527 \pm 0.104	0.573 \pm 0.100	0.627 \pm 0.129
Door	0.860 \pm 0.028	0.827 \pm 0.082	0.887 \pm 0.034
Stack	0.160 \pm 0.016	0.067 \pm 0.025	0.220 \pm 0.016

4.4 Performance improvements

As shown in Table 1, diffusion policies coupled with ICon consistently outperform or match the baselines across all 5 tasks in the RL Bench simulated environments. Notably, ICon-Diff-C achieves absolute improvements of 21.3% and 11.3% over Diff-C in the *Open Box* and *Close Microwave* tasks, respectively. In another articulated object manipulation task *Close Drawer*, the positive effects of incorporating ICon are less pronounced, but ICon-augmented policies still perform on par with or better than the baselines. In contrast, Crossway-Diff-C underperforms Diff-C and ICon-Diff-C across all three articulated object manipulation tasks. In the *Take Lid off Saucepan* task, ICon-Diff-C and Crossway-Diff-C both exhibit higher success rates than Diff-C, with ICon-Diff-C showing more

substantial improvements. Likewise, ICon-Diff-T surpasses Diff-T with an absolute improvement of 13.3%. In the long-horizon *Put Rubbish in Bin* task, all CNN-based diffusion policies fail to succeed, whereas ICon-Diff-T remains better than Diff-T.

As displayed in Table 2, ICon-Diff-C outperforms both Diff-C and Crossway-Diff-C across all tasks. In the *Open Door* task, Diff-C underperforms ICon-Diff-C but outperforms Crossway-Diff-C, aligning with earlier experimental results on articulated object manipulation tasks in the RL Bench environments. In the *Stack* task, ICon-Diff-C surpasses both Diff-C and Crossway-Diff-C with improvements of 6.0% and 15.3%, respectively. Overall, integrating ICon into diffusion policies leads to improved performance across all 8 manipulation tasks.

Table 3: Results of few-shot policy transfer across different robots on the Robosuite benchmark. Policies are transferred from a source robot to a target robot, with task success rates reported for each robot and learning algorithm. Success rates are displayed following the same format as in Table 1 and Table 2.

Task	Source Robot		Target Robot			
	Franka (Default Gripper)		Kinova (Robotiq85)		IIWA (Robotiq140)	
	Diff-C	ICon-Diff-C	Diff-C	ICon-Diff-C	Diff-C	ICon-Diff-C
Lift	0.527 ± 0.104	0.627 ± 0.129	0.233 ± 0.066	0.260 ± 0.102	0.060 ± 0.016	0.100 ± 0.125
Stack	0.160 ± 0.016	0.220 ± 0.016	0.007 ± 0.009	0.053 ± 0.025	0.007 ± 0.009	0.047 ± 0.025

4.5 Transferability across robots

Here, we evaluate the transferability of ICon-augmented policies across 3 robots from the Robosuite benchmark, where variations come from both robotic arms (Franka, Kinova, IIWA) and grippers (Franka Default Gripper, Robotiq85, Robotiq140). We initially pre-train policies on data collected from a source robot, and then fine-tune them using a smaller dataset collected from a target robot. Results in Table 3 show that ICon enhances the performance of the base policy across all three robots in both the *Lift* and *Stack* tasks. We also find that policies are more effectively transferred to the Kinova robot than to the IIWA robot, which we believe is because of the appearance similarity between the Kinova and the source Franka robot.

4.6 Training stability

A key strength of ICon is to maintain good training stability during end-to-end policy learning. For a quantitative measure, we train each policy for an equal number of epochs with checkpoints saved every 50 epochs, and report the average of the top-10 success rates as well as the overall maximum success rate for the *Open Door* task. Results are visualized in Figure 4, with dark and light colors representing maximum and average success rates, respectively. The accompanying percentages stand for the relative drop from the maximum to the average performance. We see that when maximum performances are comparable, Crossway-Diff-C exhibits the largest gap between maximum and average success rates, indicating that the auxiliary reconstruction loss hinders the training stability of the base policy. In contrast, ICon-Diff-C shows superior training stability by maintaining a relatively higher average performance throughout the training process. This suggests that ICon enables the base policy to learn more robust and consistent behaviors from pixel observations.

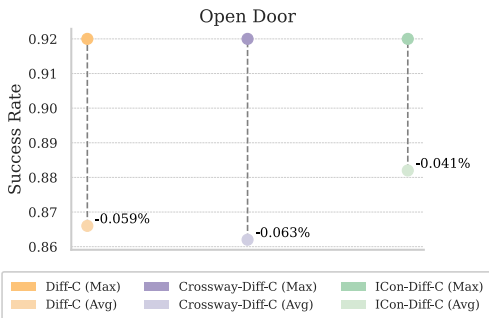


Figure 4: Comparison of training stability based on maximum and average performance during the training process.

4.7 Ablation study

We evaluate how each key component of ICon contributes to its overall performance. Specifically, we conduct ablation studies on: (i) the masking threshold β ; (ii) the number of agent keys N_a and environment keys N_e used in computing the contrastive loss; and (iii) the key sampling and loss fusion strategies. These experiments are performed on the *Open Door*, *Close Microwave*, and *Open Box* tasks, respectively. A summary of the results is presented in Figure 5.

We note that choosing either $\beta < 0.5$ or $\beta > 0.5$ substantially impairs model performance, indicating that assigning equal weights (0.5) to agent-specific and environment-specific pixels during agent mask propagation yields the most accurate approximation of token-level masks. Next, we find that increasing the number of sampled keys beyond a certain point markedly extends training time. While a larger number of keys enables more effective disentanglement, a practical trade-off is achieved by setting $N_a = 10$ and $N_e = 50$. Finally, we observe that omitting Multi-Level Contrast (MLC) results in a noticeable decline in performance, which we attribute to the insufficient disentangling of intermediate representations in the vision transformer. A more significant performance degradation occurs when random sampling is applied in place of FPS for key sampling, likely due to the reduced expressivity of the sampled keys.

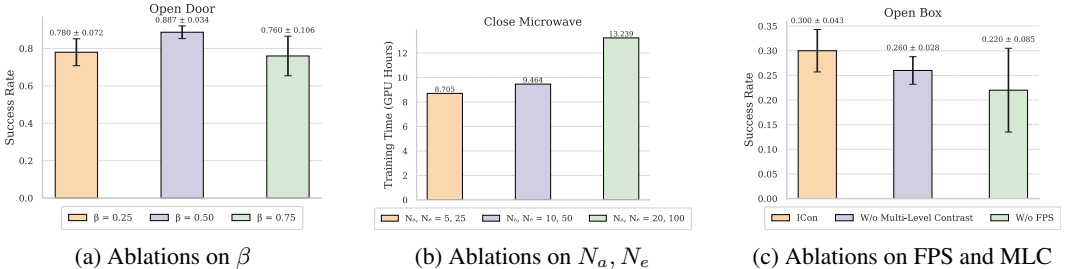


Figure 5: Summary of ablation experiments on (a) the masking threshold β , (b) the number of agent keys N_a and environment keys N_e , and (c) the use of Farthest Point Sampling (FPS) and Multi-Level Contrast (MLC).

5 Limitations

While our simulation experiments demonstrate that ICon improves the base policy across a variety of manipulation tasks, our work has several limitations. First, the farthest point sampling process incurs substantial computational overhead during forward propagation, making ICon inefficient for policy training on large-scale manipulation datasets. Second, our experiments are confined to simulation, and we have not yet evaluated our method in real-world settings due to limited hardware resources.

6 Discussion and future work

In this work, we investigate the benefits of grounding bodily awareness in visual representations and introduce ICon, a contrastive learning framework for extracting agent-centric representations from pixel observations. We demonstrate that policies augmented with ICon consistently achieve performance improvements across a diversity of manipulation tasks and can be effectively few-shot transferred across robots with different morphologies and configurations. In our future work, we plan to evaluate our method in complex real-world settings, where additional noise and distractors are present in the environments. Additionally, we hope to further enhance the learned agent-centric representations and develop more effective ones to enable zero-shot policy transfer.

7 Acknowledgements

We thank Tianyu Wu for his assistance in developing the project website. We thank Sirui Cheng for his help with the simulation experiments. We also thank Dr. Chaoyang Song for the insightful discussions and thoughtful guidance.

References

- [1] S. Amir, Y. Gandelsman, S. Bagon, and T. Dekel. Deep vit features as dense visual descriptors. *arXiv preprint arXiv:2112.05814*, 2021.
- [2] J. L. Bermúdez. Bodily awareness and self-consciousness. In Shaun Gallagher, editor, *The Oxford Handbook of the Self*, pages 157–179. Oxford University Press, 2011.
- [3] M. Caron, H. Touvron, I. Misra, H. Jégou, J. Mairal, P. Bojanowski, and A. Joulin. Emerging properties in self-supervised vision transformers. In *Proceedings of the IEEE/CVF International Conference on Computer Vision*, pages 9650–9660, Montreal, Canada, 2021.
- [4] T. Chen, S. Kornblith, M. Norouzi, and G. Hinton. A simple framework for contrastive learning of visual representations. In *Proceedings of the 37th International Conference on Machine Learning*, pages 1597–1607, Vienna, Austria, 2020.
- [5] C. Chi, Z. Xu, S. Feng, E. Cousineau, Y. Du, B. Burchfiel, R. Tedrake, and S. Song. Diffusion policy: Visuomotor policy learning via action diffusion. In *Proceedings of Robotics: Science and Systems*, Daegu, Republic of Korea, 2023.
- [6] S. Chopra, R. Hadsell, and Y. LeCun. Learning a similarity metric discriminatively, with application to face verification. In *Proceedings of the IEEE Computer Society Conference on Computer Vision and Pattern Recognition*, pages 539–546, San Diego, CA, USA, 2005.
- [7] S. Dasari and A. Gupta. Transformers for one-shot visual imitation. In *Proceedings of the 5th Conference on Robot Learning*, pages 2071–2084, London, UK, 2021.
- [8] A. Dosovitskiy, L. Beyer, A. Kolesnikov, D. Weissenborn, X. Zhai, T. Unterthiner, M. Dehghani, M. Minderer, G. Heigold, S. Gelly, J. Uszkoreit, and N. Houlsby. An image is worth 16x16 words: Transformers for image recognition at scale. *arXiv preprint arXiv:2010.11929*, 2020.
- [9] L. Fu, H. Huang, G. Datta, L. Y. Chen, W. C. Panitch, F. Liu, H. Li, and K. Goldberg. In-context imitation learning via next-token prediction. *arXiv preprint arXiv:2408.15980*, 2024.
- [10] J. J. Gibson. The senses considered as perceptual systems. 1966.
- [11] J. J. Gibson. A theory of direct visual perception. *Vision and Mind: selected readings in the philosophy of perception*, pages 77–90, 2002.
- [12] K. Gmelin, S. Bahl, R. Mendonca, and D. Pathak. Efficient rl via disentangled environment and agent representations. *arXiv preprint arXiv:2309.02435*, 2023.
- [13] M. Gutmann and A. Hyvärinen. Noise-contrastive estimation: A new estimation principle for unnormalized statistical models. In *Proceedings of the 13th International Conference on Artificial Intelligence and Statistics*, pages 297–304, Sardinia, Italy, 2010.
- [14] K. He, X. Zhang, S. Ren, and J. Sun. Deep residual learning for image recognition. In *Proceedings of the IEEE/CVF Conference on Computer Vision and Pattern Recognition*, pages 770–778, Las Vegas, NV, USA, 2016.
- [15] K. He, H. Fan, Y. Wu, S. Xie, and R. Girshick. Momentum contrast for unsupervised visual representation learning. In *Proceedings of the IEEE/CVF Conference on Computer Vision and Pattern Recognition*, pages 9729–9738, Seattle, WA, USA, 2020.
- [16] J. Ho, A. Jain, and P. Abbeel. Denoising diffusion probabilistic models. In *Proceedings of the 34th Conference on Neural Information Processing Systems*, pages 6840–6851, Vancouver, Canada, 2020.
- [17] E. S. Hu, K. Huang, O. Rybkin, and D. Jayaraman. Know thyself: Transferable visual control policies through robot-awareness. *arXiv preprint arXiv:2107.09047*, 2021.
- [18] S. James, Z. Ma, D. R. Arrojo, and A. J. Davison. Rlbench: The robot learning benchmark and learning environment. *IEEE Robotics and Automation Letters*, 5(2):3019–3026, 2020.

- [19] S. Karamcheti, S. Nair, A. S. Chen, T. Kollar, C. Finn, D. Sadigh, and P. Liang. Language-driven representation learning for robotics. In *Proceedings of Robotics: Science and Systems*, Daegu, Republic of Korea, 2023.
- [20] A. Kirillov, E. Mintun, N. Ravi, H. Mao, C. Rolland, L. Gustafson, T. Xiao, S. Whitehead, A. C. Berg, W. Lo, P. Dollár, and R. Girshick. Segment anything. In *Proceedings of the IEEE/CVF International Conference on Computer Vision*, pages 4015–4026, Paris, France, 2023.
- [21] I. Kostrikov, D. Yarats, and R. Fergus. Image augmentation is all you need: Regularizing deep reinforcement learning from pixels. *arXiv preprint arXiv:2004.13649*, 2020.
- [22] M. Laskin, A. Srinivas, and P. Abbeel. Curl: Contrastive unsupervised representations for reinforcement learning. In *Proceedings of the 37th International Conference on Machine Learning*, pages 5639–5650, Vienna, Austria, 2020.
- [23] S. Lee, Y. Wang, H. Etukuru, H. J. Kim, N. M. M. Shafiullah, and L. Pinto. Behavior generation with latent actions. In *Proceedings of the 41st International Conference on Machine Learning*, pages 26991–27008, Vienna, Austria, 2024.
- [24] S. Levine, C. Finn, T. Darrell, and P. Abbeel. End-to-end training of deep visuomotor policies. *Journal of Machine Learning Research*, 17(39):1–40, 2016.
- [25] X. Li, V. Belagali, J. Shang, and M. S. Ryoo. Crossway diffusion: Improving diffusion-based visuomotor policy via self-supervised learning. In *Proceedings of the IEEE International Conference on Robotics and Automation*, pages 16841–16849, Yokohama, Japan, 2024.
- [26] A. Mandlekar, D. Xu, J. Wong, S. Nasiriany, C. Wang, R. Kulkarni, L. Fei-Fei, S. Savarese, Y. Zhu, and R. Martín-Martín. What matters in learning from offline human demonstrations for robot manipulation. *arXiv preprint arXiv:2108.03298*, 2021.
- [27] S. Nair, A. Rajeswaran, V. Kumar, C. Finn, and A. Gupta. R3m: A universal visual representation for robot manipulation. In *Proceedings of the 6th Conference on Robot Learning*, pages 892–909, Auckland, New Zealand, 2022.
- [28] A. V. D. Oord, Y. Li, and O. Vinyals. Representation learning with contrastive predictive coding. *arXiv preprint arXiv:1807.03748*, 2018.
- [29] A. Pore, R. Muradore, and D. Dall’Alba. Dear: Disentangled environment and agent representations for reinforcement learning without reconstruction. In *Proceedings of the IEEE/RSJ International Conference on Intelligent Robots and Systems*, pages 650–655, Abu Dhabi, UAE, 2024.
- [30] C. R. Qi, L. Yi, H. Su, and L. J. Guibas. Pointnet++: Deep hierarchical feature learning on point sets in a metric space. In *Proceedings of the 31st International Conference on Neural Information Processing Systems*, pages 5099–5108, Long Beach, CA, USA, 2017.
- [31] A. Radford, J. W. Kim, C. Hallacy, A. Ramesh, G. Goh, S. Agarwal, G. Sastry, A. Askell, P. Mishkin, J. Clark, G. Krueger, and I. Sutskever. Learning transferable visual models from natural language supervision. In *Proceedings of the 38th International conference on machine learning*, pages 8748–8763, 2021.
- [32] I. Radosavovic, T. Xiao, S. James, P. Abbeel, J. Malik, and T. Darrell. Real-world robot learning with masked visual pre-training. In *Proceedings of the 7th Conference on Robot Learning*, pages 416–426, Atlanta, GA, USA, 2023.
- [33] N. Ravi, V. Gabeur, Y. Hu, R. Hu, C. Ryali, T. Ma, H. Khedr, R. Rädle, C. Rolland, L. Gustafson, E. Mintun, J. Pan, K. V. Alwala, N. Carion, C. Wu, R. Girshick, P. Dollár, and C. Feichtenhofer. Sam 2: Segment anything in images and videos. *arXiv preprint arXiv:2408.00714*, 2024.
- [34] O. Ronneberger, P. Fischer, and T. Brox. U-net: Convolutional networks for biomedical image segmentation. In *Proceedings of the International Conference on Medical Image Computing and Computer-Assisted Intervention*, pages 234–241, Munich, Germany, 2015.

- [35] F. Schroff, D. Kalenichenko, and J. Philbin. Facenet: A unified embedding for face recognition and clustering. In *Proceedings of the IEEE Conference on Computer Vision and Pattern Recognition*, pages 815–823, Boston, MA, USA, 2015.
- [36] P. Sermanet, C. Lynch, Y. Chebotar, J. Hsu, E. Jang, S. Schaal, S. Levine, and Google Brain. Time-contrastive networks: Self-supervised learning from video. In *Proceedings of the IEEE International Conference on Robotics and Automation*, pages 1134–1141, Brisbane, Australia, 2018.
- [37] N. M. Shafiullah, Z. Cui, A. A. Altanzaya, and L. Pinto. Behavior transformers: Cloning k modes with one stone. In *Proceedings of the 36th Conference on Neural Information Processing Systems*, pages 22955–22968, New Orleans, LA, USA, 2022.
- [38] Kihyuk Sohn. Improved deep metric learning with multi-class n-pair loss objective. In *Proceedings of the 30th International Conference on Neural Information Processing Systems*, page 1857–1865, Red Hook, NY, USA, 2016.
- [39] G. Soter, A. Conn, H. Hauser, and J. Rossiter. Bodily aware soft robots: integration of proprioceptive and exteroceptive sensors. In *Proceedings of the IEEE International Conference on Robotics and Automation*, pages 2448–2453, Brisbane, Australia, 2018.
- [40] A. Vaswani, N. Shazeer, N. Parmar, J. Uszkoreit, L. Jones, A. N. Gomez, Ł. Kaiser, and I. Polosukhin. Attention is all you need. In *Proceedings of the 31st International Conference on Neural Information Processing Systems*, pages 6000–6010, Long Beach, CA, USA, 2017.
- [41] X. Wang, K. Zhao, R. Zhang, S. Ding, Y. Wang, and W. Shen. Contrastmask: Contrastive learning to segment every thing. In *Proceedings of the IEEE/CVF Conference on Computer Vision and Pattern Recognition*, pages 11604–11613, New Orleans, LA, USA, 2022.
- [42] T. Xiao, I. Radosavovic, T. Darrell, and J. Malik. Masked visual pre-training for motor control. *arXiv preprint arXiv:2203.06173*, 2022.
- [43] M. Xu, Z. Xu, C. Chi, M. Veloso, and S. Song. Xskill: Cross embodiment skill discovery. In *Proceedings of the 7th Conference on Robot Learning*, pages 3536–3555, Atlanta, GA, USA, 2023.
- [44] D. Yarats, R. Fergus, A. Lazaric, and L. Pinto. Mastering visual continuous control: Improved data-augmented reinforcement learning. *arXiv preprint arXiv:2107.09645*, 2021.
- [45] D. Yarats, A. Zhang, I. Kostrikov, B. Amos, J. Pineau, and R. Fergus. Improving sample efficiency in model-free reinforcement learning from images. In *Proceedings of the AAAI Conference on Artificial Intelligence*, pages 10674–10681, 2021.
- [46] T. Z. Zhao, V. Kumar, S. Levine, and C. Finn. Learning fine-grained bimanual manipulation with low-cost hardware. In *Proceedings of Robotics: Science and Systems*, Daegu, Republic of Korea, 2023.
- [47] J. Zhu, Y. Xia, L. Wu, J. Deng, W. Zhou, T. Qin, T. Liu, and H. Li. Masked contrastive representation learning for reinforcement learning. *IEEE Transactions on Pattern Analysis and Machine Intelligence*, 45(3):3421–3433, 2022.
- [48] Y. Zhu, J. Wong, A. Mandlekar, R. Martín-Martín, A. Joshi, S. Nasiriany, and Y. Zhu. robo-suite: A modular simulation framework and benchmark for robot learning. *arXiv preprint arXiv:2009.12293*, 2020.

A Implementation details

A.1 Data augmentation

Following Chi et al. [5], we apply random cropping to both RGB images and agent masks during training. The crop size is fixed at $3 \times 224 \times 224$ across all tasks. During inference, a static center crop of the same size is used.

A.2 Model architecture

The policy networks used in this work are built upon the Diffusion Policy [5]. We keep the overall model architecture unchanged except for the visual encoder, where we replace the ResNet [14] with a Vision Transformer (ViT) [8]. To save computing resources, we employ ViT-S with a patch size of 16 and an input image size of 224 as the visual encoder for our policy network.

A.3 Environmental setup

Details of the environment setup for RLbench and Robosuite are provided in Table 4. Note that in RLbench, robot proprioception includes arm joint positions, end-effector poses, and gripper status, whereas in Robosuite, robot proprioception consists of end-effector poses and gripper joint positions.

Table 4: Summary of task environments. **Objs**: number of objects in the scene; **Views**: number of viewpoints; **Img-Size**: image size; **P-D**: robot proprioception dimension; **A-D**: action dimension; **Controller**: robotic arm controller; **Steps**: maximum number of rollout steps.

	Objs	Views	Img-Size	P-D	A-D	Controller	Steps
Close Microwave	1	2	$3 \times 256 \times 256$	14	7	IK Pose	150
Close Drawer	1	2	$3 \times 256 \times 256$	14	7	IK Pose	200
Open Box	1	2	$3 \times 256 \times 256$	14	7	IK Pose	200
Take Lid off Saucepan	2	2	$3 \times 256 \times 256$	14	7	IK Pose	200
Put Rubbish in Bin	4	2	$3 \times 256 \times 256$	14	7	IK Pose	300
Lift	1	2	$3 \times 256 \times 256$	9	7	OSC Pose	200
Door	1	2	$3 \times 256 \times 256$	9	7	OSC Pose	300
Stack	2	2	$3 \times 256 \times 256$	9	7	OSC Pose	300

A.4 Training

We train our policy networks, ICon-Diff-C and ICon-Diff-T, using 3 training seeds (0, 42, and 100) and a batch size of 64. For each task, all policies are trained for 600 epochs on a single Nvidia GeForce RTX 3090 GPU, while in cross-robot transfer settings, the pre-trained policies are fine-tuned on the target robotic data for an additional 300 epochs. All other training configurations follow the settings described in the original codebase of Diffusion Policy [5]. The corresponding training time is summarized in Table 5.

Table 5: Training time measured in GPU hours for each task.

	ICon-Diff-C	ICon-Diff-T
Close Microwave	9.46	9.57
Close Drawer	11.50	13.02
Open Box	17.28	17.47
Take Lid off Saucepan	8.69	12.13
Put Rubbish in Bin	15.06	15.88
Lift	9.11	-
Door	16.48	-
Stack	11.76	-

B Visualization of learned representations

After training the vision transformer end-to-end with the policy network from scratch, we visualize the attention maps from the final layer of the vision transformer across several tasks. As shown in Figure 6, unlike the dispersed attention patterns exhibited by the baseline method, our contrastive learning approach encourages the vision transformer to focus on the agent’s body rather than the entire scene. This confirms that the learned representations are agent-centric and carry body-relevant information about the robotic agent.

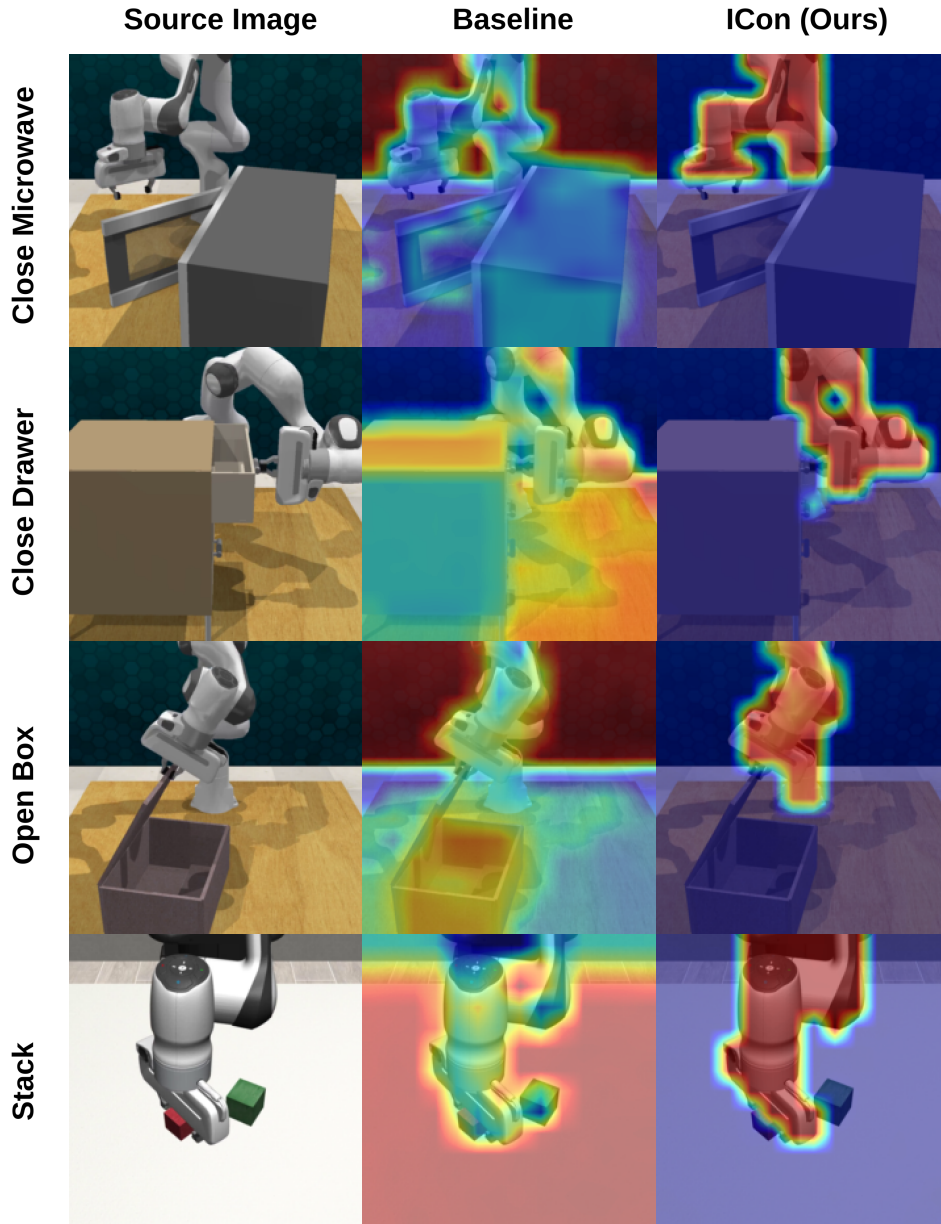


Figure 6: Visualization of representations learned by different algorithms across several tasks. For each task, we show the original image alongside the feature maps produced by different algorithms. Each feature map is computed by averaging the attention maps from all heads in the final layer of the vision transformer, with the [CLS] token as the query.

C Computational overhead

We compare the training time of different key sampling strategies for inter-token contrastive learning on the *Close Microwave* task. As shown in Table 6, the training time with random sampling increases only slightly as the number of sampled keys grows. In contrast, the training time with FPS rises substantially, indicating that FPS introduces significantly higher computational overhead than random sampling under heavier sampling loads.

Table 6: Training time (GPU hours) for random sampling and FPS under different numbers of agent and environment keys.

Sampling Method	Agent & Environment Keys		
	5 & 25	10 & 50	20 & 100
Random Sampling	7.253	7.328	7.455
FPS	8.705	9.464	13.239

D Pseudocode

Algorithm 2 Inter-token Contrast (Icon)

- 1: **Input:** an RGB image $\mathcal{I} \in \mathbb{R}^{H \times W \times 3}$, an agent mask $\mathcal{M} \in \mathbb{R}^{H \times W}$, a vision transformer $\mathcal{E}(\cdot)$ with patch size P and embedding dimension D , number of agent-specific keys N_a , number of environment-specific keys N_e
 - 2: **Output:** a contrastive loss $\mathcal{L}_{\text{Icon}}$
 - 3: $[\mathcal{F}_{\text{cls}}, \mathcal{F}] \leftarrow \mathcal{E}(\mathcal{I})$
 - 4: $\mathcal{F}_{\text{map}} = \{f_{k,l} \in \mathbb{R}^D\}_{k=1,l=1}^{H/P,W/P} \leftarrow \text{Reshape}(\mathcal{F})$
 - 5: $\mathcal{P}_{\text{mask}} = \{p_{k,l} \in \mathbb{R}^D\}_{k=1,l=1}^{H/P,W/P} \leftarrow \text{Patchify}(\mathcal{M})$
 - 6: $\mathcal{M}_{\text{token}} = \{m_{k,l} \in \{0,1\}\}_{k=1,l=1}^{H/P,W/P} \leftarrow \text{Threshold}(\mathcal{P}_{\text{mask}})$ ▷ Equation 2
 - 7: $q_a, q_e \leftarrow \text{Average}(\mathcal{F}_{\text{map}}, \mathcal{M}_{\text{token}}), \text{Average}(\mathcal{F}_{\text{map}}, 1 - \mathcal{M}_{\text{token}})$ ▷ Equation 3
 - 8: $\mathcal{K}_a, \mathcal{K}_e \leftarrow \text{FPS}(\mathcal{F}_{\text{map}}, \mathcal{M}_{\text{token}}, N_a), \text{FPS}(\mathcal{F}_{\text{map}}, 1 - \mathcal{M}_{\text{token}}, N_e)$ ▷ Algorithm 1
 - 9: $\mathcal{L}_a, \mathcal{L}_e \leftarrow \mathcal{L}_{\text{InfoNCE}}(q_a, \mathcal{K}_a, \mathcal{K}_e), \mathcal{L}_{\text{InfoNCE}}(q_e, \mathcal{K}_e, \mathcal{K}_a)$ ▷ Equation 1
 - 10: $\mathcal{L}_{\text{Icon}} \leftarrow \mathcal{L}_a + \mathcal{L}_e$
 - 11: **return** $\mathcal{L}_{\text{Icon}}$
-